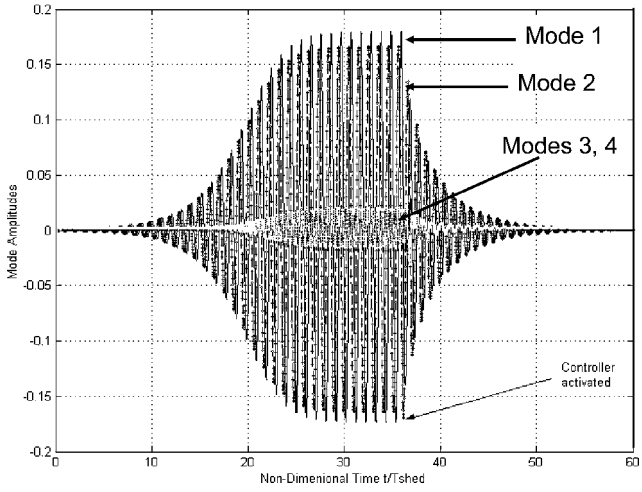

Fig. 1 Flow response to proportional feedback, $K_p = 3.0$.

Conclusions

A simple approach to control the von Kármán vortex street behind a two-dimensional circular cylinder based on the proportional feedback of the estimate of just the first POD mode has been developed. A stability analysis of this control law was conducted after linearization about the desired equilibrium point (origin) and conditions for controllability and asymptotic stability were developed. The control approach, applied to the four-mode cylinder wake POD model at a Reynolds number of 100 stabilizes the wake for a proportional gain above 1.6. Whereas the controller uses only the estimated amplitude of the first mode, all four modes are stabilized. This suggests that the higher-order modes are caused by a secondary instability. Thus, they are suppressed once the primary instability is controlled. The control approach will be further examined to observe its sensitivity to time delays, actuator limitations, modeling and estimation errors, and sensor noise.

References

[1]Albarede, P., and Provansal, M., "Quasi-Periodic Cylinder Wakes and the Ginzburg–Landau Model," *Journal of Fluid Mechanics*, Vol. 291, 1995, pp. 191–222.

[2]Roussopoulos, K., "Feedback Control of Vortex Shedding at Low Reynolds Numbers," *Journal of Fluid Mechanics*, Vol. 248, 1993, pp. 267–296.

[3]Park, D. S., Ladd, D. M., and Hendricks, E. W., "Feedback Control of von Kármán Vortex Shedding Behind a Cylinder at Low Reynolds Numbers," *Physics of Fluids*, Vol. 6, No. 7, 1994, pp. 2390–2405.

[4]Monkewitz, P. A., "Modeling of Self-Excited Wake Oscillations by Amplitude Equations," *Experimental Thermal and Fluid Science*, Vol. 12, 1996, pp. 175–183.

[5]Blevins, R., *Flow Induced Vibration*, 2nd ed., Van Nostrand Reinhold, New York, 1990, pp. 54–58.

[6]Gillies, E. A., "Low-Dimensional Characterization and Control of Non-Linear Wake Flows," Ph.D. Dissertation, Faculty of Engineering, Univ. of Glasgow, Glasgow, Scotland, U.K., June 1995.

[7]Gillies, E. A., "Low-Dimensional Control of the Cylinder Wake," *Journal of Fluid Mechanics*, Vol. 371, 1998, pp. 157–178.

[8]Holmes, P., Lumley, J. L., and Berkooz, G., *Turbulence, Coherent Structures, Dynamical Systems and Symmetry*, Cambridge Univ. Press, Cambridge, England, U.K., 1996, pp. 86–127.

[9]Siegel, S., Cohen, K., Smith, D., and McLaughlin, T., "Observability Conditions for POD Modes in a Circular Cylinder Wake," *Bulletin of the American Physical Society*, Vol. 47, No. 10, 2002, pp. 65, 66.

[10]Nijmeijer, H., and van der Schaft, A. J., *Nonlinear Dynamical Control Systems*," Springer-Verlag, New York, 1990, pp. 73–113.

[11]Glendinning, P., *Stability, Instability and Chaos: An Introduction to the Theory of Non-Linear Differential Equations*, Cambridge Texts in Applied Mathematics, Cambridge Univ. Press, New York, 1994, pp. 25–53.

[12]Strogatz, S. H., "Nonlinear Dynamics and Chaos—With Applications to Physics, Chemistry and Engineering," *Studies in Nonlinearity*, Addison–Wesley, Reading, MA, 1994, pp. 145–181.

A. Plotkin
Associate Editor

A Mechanism for Flame Acceleration in Narrow Tubes

James D. Ott*
Combustion Research and Flow Technology, Dublin, Pennsylvania 18917
Elaine S. Oran†
U.S. Naval Research Laboratory, Washington, D.C. 20375
and
John D. Anderson Jr.‡
National Air and Space Museum, Smithsonian Institution, Washington, D.C. 20560-0312

Introduction

THIS Note describes a process by which a low-speed, laminar flame and the laminar boundary layer created by this flame interact dynamically to increase the flame propagation velocity exponentially.[1,2] The condition for this flame acceleration is that the flame propagates in a narrow enough channel with heated walls. This phenomenon has potential applications to micropropulsion, and it may describe aspects of explosion initiation in fissures in condensed-phase energetic materials and deflagration-to-detonation transition.

The key element is the presence of the boundary layer that develops along the walls ahead of the flame. This boundary layer develops as the flame propagates, and it is due to fluid motion in unburned material that is induced by expansion of the heated material at the flame front. The fluid motion that develops in the unreacted material ahead of the flame is caused by the expansion of the gas as it burns and acts like a piston. If the flame is accelerating, it generates pressure waves; if it is decelerating, it generates expansion waves. (There may also be a relatively smaller boundary layer behind a weak shock that could arise as a spark lights the flame, but this is much smaller than the boundary layer developing as the flame itself propagates and generates fluid motion ahead of it.)

Figure 1 shows the basic geometry: a flame propagating from the closed end toward the open end of a channel. There is a considerable body of work in the combustion literature on flow instabilities and how they affect the evolution of flames in tubes. There is the relatively early work on this geometrical configuration, for example, Refs. 3–5, in which flames were ignited by sparks and propagated for a time as laminar flames before becoming turbulent. In some cases, the flames oscillated and even reversed direction for a time before resuming movement toward the open end of the channel. There are recent measurements reported on flame propagation in narrow channels (less than 1 cm height) in which the flame accelerated and there was a transition to detonation (G. O. Thomas, private communication). In other recent experimental studies[6,7] with configurations related to Fig. 1, the width, length, and mixture composition of the gases were varied and the observed oscillation frequency was related to the acoustic properties of the channel. Related theoretical and

Received 1 November 2002; revision received 11 March 2003; accepted for publication 11 March 2003.

*Research Scientist, 174 North Main Street, Building 3, P.O. Box 1150. Member AIAA.

†Senior Scientist for Reactive Flow Physics, Laboratory for Computational Physics and Fluid Dynamics (Code 6404). Fellow AIAA.

‡Curator for Aeronautics, Aeronautics Division, Independence Avenue at 6th Street, Southwest. Fellow AIAA.

Table 1 Material, chemical, and flame properties

Property	Value	Definition
	Input	
T_0	293 K	Initial temperature
P_0	1.33×10^4 J/m^3	Initial pressure
ρ_0	1.58×10^{-1} kg/m^3	Initial density
Y_0	1	Initial composition
γ	1.25	Adiabatic index
M	29	Molecular weight
A	1×10^9 m^3/kg/s	Pre-exponential factor
Q	$29.3\,R\,T_0$	Activation energy
q	$35.0\,R\,T_0/M$	Chemical energy release
ν_0, κ_0, D_0	1.3×10^{-6}	Transport constants
	Output	
T_b	2340 K	Flame temperature
ρ_b	1.98×10^{-2} kg/m^3	Flame density
S_l	$\simeq 1.31$ m/s	Laminar flame speed
x_l	$\simeq 0.023$ cm	Laminar flame thickness

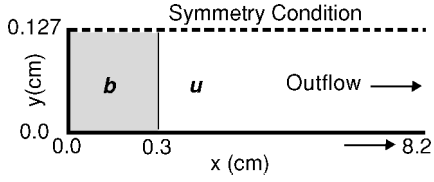

Fig. 1 Schematic diagram of computational setup and initial conditions.

numerical studies for a similar geometry include one-dimensional studies of the effects of acoustic waves in the channel, and how these waves are related to flame oscillations.[7] Theoretical and numerical studies[8,9] have been performed of a Poiseuille flow with a flame in a tube. These did not solve the full Navier–Stokes equations (they assumed constant density, for example) but looked at the effects of flame propagation with both adiabatic and nonadiabatic walls and, later, with the effects of heat losss to the walls. In other recent work,[10,11] the evolution of a flame in flow that produces a shock and boundary layers ahead of the flame has been studied. Most of this work, however, applies to somewhat different physical conditions from those studied here, often considering relatively large channels, constant density combustion, or emphasis on events occurring much later in the evolution of the flow than those considered here.

Physical Model and Numerical Method

Consider a two-dimensional channel filled with premixed acetylene and air, shown schematically in Fig. 1. The propagation of the flame down this channel is given by the solution of the reactive compressible Navier–Stokes equations; see Ref. 1 or 2 for details of equations and solution approach. These equations include models for chemical reactions and subsequent energy release, molecular diffusion, thermal conduction, and viscosity. Let the flame be initiated by a planar discontinuity in temperature and density located at 0.3 cm from the closed end of the channel (Fig. 1). The burned material to the left of the discontinuity is at the adiabatically burned conditions given in Table 1. The material to the right is unburned. A symmetry condition is used at the top of the computational domain, and gravitational terms are neglected on the assumption that they should not be a major effect in such narrow channels.

For simplicity, the chemical reactions are modeled by a single-step, reduced model for combustion of a low-pressure, stoichiometric, acetylene–air mixture at 1.33×10^4 Pa (0.132 atm) and 293 K (Refs. 12–14). The chemical reactions are described by first-order Arrhenius kinetics expressed as $\mathrm{d}Y/\mathrm{d}t = -A\rho Y \exp(-Q/RT)$, where Y is the mass fraction of the reactant, A is the preexponential factor, and Q is the activation energy. The reaction rate is proportional to ρ to account for the binary nature of chemical reactions taking place in real combustion systems. The energy release per unit volume is $\mathrm{d}E/\mathrm{d}t = -q\rho\mathrm{d}Y/\mathrm{d}t$, where q is the total chemical energy released per gram. We assume that there is a similar temperature dependence for the kinematic viscosity, diffusion, and heat conduction, $\nu = \nu_0 T^n/\rho$, $D = D_0 T^n/\rho$, and $K/\rho C_p = \kappa_0 T^n/\rho$, where the $\nu_0 = D_0 = \kappa_0$ are constants and $C_p = \gamma R/M(\gamma - 1)$ is the specific heat at constant pressure. The nondimensional Lewis, Prandtl, and Schmidt numbers, $Le = K/\rho C_p D = \kappa_0/D_0$, $Pr = \rho C_p \nu/K = \nu_0/\kappa_0$, and $Sc = \nu/D = \nu_0/D_0$, are unity and independent of thermodynamic conditions.

The properties of the chemical and thermophysical input data were determined to produce a model that gives the physically correct flame (and detonation) properties of this mixture over a range of temperatures and pressures. Values of input quantities used in the computation are given in Table 1. Note that the computation uses a model for the chemical and diffusive transport reactions. When the input values for this model are considered individually, they do not seem to be very accurate. What is important, however, is that the individual parameters are physically reasonable values and that the combination of parameters, when used in the test numerical simualtions, reproduce the accepted values of the flame and detonation properties. These "accepted values" have been determined from experiments and computations using better chemical and transport models, and these are given in Table 1.

The computational model used a high-order flux-corrected transport algorithm[15] to solve the compressible fluid-dynamics equations. Viscous, conduction, and mass diffusion terms were added as source terms. The equations and the solution procedure are described in detail elsewhere, for example, Refs. 16 and 17. Ott[1] and Ott et al.[2] provide detailed information on extensive tests of the procedure. The chemical reaction terms were computed separately and incorporated by time-step splitting.[15] Because the fluid dynamics is computed with a high-order numerical method, the boundary conditions are computed by a characteristic method.[18,19] Ott[1] and Ott et al.[2] give extensive details of the derivation of the rather complex boundary conditions for the inflow, outflow, adiabatic-wall, and isothermal-wall conditions used here. These will be describe in a more detailed paper that is in preparation.

For some of the cases described here, the walls were adiabatic. This means that their temperature was assumed to be that of the gas inside the channel just above the walls. This is the limiting case of walls adjacent to a flame becoming quickly heated to the temperature of the hot gas, but the heat not being transmitted quickly to the walls ahead of the flame. For simulations in another limit, cold walls at fixed temperature, the wall at the closed end and on the x axis from 0.0 to 0.3 cm was adiabatic and the walls for $x > 0.3$ cm was isothermal.

Extensive resolution tests were done in which the computational cell sizes were varied in the range from 1×10^{-5} to 4×10^{-5} m. This corresponds to from 25 to 6 computational cells in a one-dimensional, undriven flame front. The results shown subsequently were computed with $\Delta x = 2.0 \times 10^{-5}$ m and $\Delta y = 1.0 \times 10^{-5}$ m.

From a computational point of view, using a fully compressible, explicit algorithm would seem to waste computational resources. For example, to compute a relatively low-velocity propagating flame, it might be best to use an implicit algorithm that would filter out effects of the sound waves or an adaptive grid that would concentrate small computational cells where there is a front or boundary layer. Techniques for all of these have been developed and can now be applied quite successfully. [In fact, the specific calculations shown here were also performed with an entirely different lower-order Riemann-solver-based method, using adaptive mesh refinement, to verify the phenomena observed described later (A. M. Khokhlov, private communication).]

Because the computations shown here are a first result of what might be a newly observed mechanism, and because they will lead to much more complex studies in compressible flows involving high-speed turbulent flames, shocks, and detonations, a number of apparently advantageous numerical short cuts were not taken. Furthermore, retaining the full sound spectrum has allowed accurate analyses of the effects of pressure and sound waves, allowing an accurate computation of the pressure jump across the propagating flame and the pressure gradients ahead of the flame.

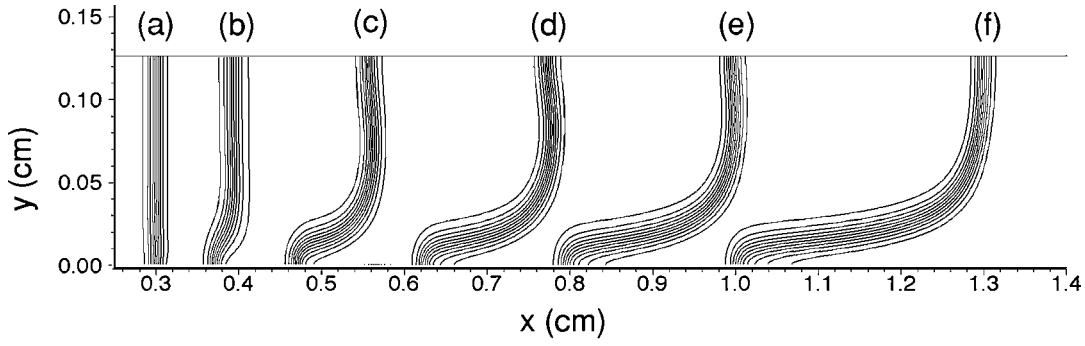

Fig. 2 Adiabatic wall; composite of temperatures at the flame front at selected early times (a–f): 0.02138, 0.10798, 0.26006, 0.39012, 0.49843, and 0.60671 ms. Contours are evenly spaced values of temperature, ranging from 400 K on the right to 2400 K on the left.

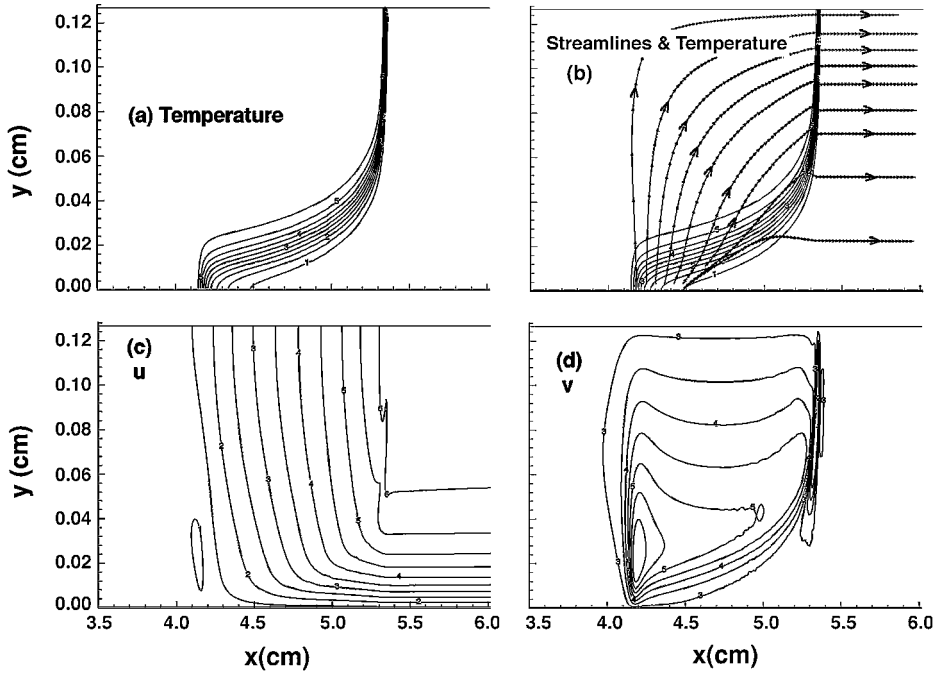

Fig. 3 Adiabatic walls; selected contours at 1.277 ms: a) temperature (ranges from 400 K on the right to 2400 K on the left), b) instantaneous streamlines superimposed on temperature, c) u (moving from left to right at the top of the figure, −600 to 9400 cm/s), and d) v (from −500 to 850 cm/s).

Results

High-Temperature Walls and Flame Acceleration

First consider how the temperature profiles develop from the initial conditions, as shown in Fig. 2. As an initially planar flame begins to propagate down the channel, it induces a flow ahead of it, and this creates the boundary layer along the wall. Figure 2 shows the boundary layer growing in time, and it continues to grow through the course of the simulation. Note that the large distortion in aspect ratio of the profiles in Fig. 2 emphasizes the structure in the y direction.

More details of the solution at a considerably later time, 1.277 ms, are shown in Figs. 3. The flame structure becomes continuously more distorted as it moves along the wall. This distortion occurs because the flow velocity in the boundary layer is less than the flow along the centerline, so that different portions of the laminar flame are moving into different background flow environments. There are several points to note here. First, as shown in the temperature contours in Fig. 3a, the flame has broadened in the boundary layer and become thinner in the middle of the channel. Second, as shown by the instantaneous streamlines and temperature contours in Fig. 3b, after the material in the boundary layer burns, it expands upward behind the flame front. The result is a fountain or upwelling of hot, fully reacted material. The upward fountain, which is perpendicular to the direction of propagation of the flame, occurs because that is the only direction it can expand: It cannot expand downward because of the wall, and it cannot expand very far to the left because it is essentially bounded by a wall of burned gas. Most of this reacted gas expands upward, where, by the symmetry condition at the centerline, it must turn, and it can only turn toward the flame front. This is also seen in the velocity contours in Fig. 3d.

Histories of the position of the two-dimensional flame at the centerline, R_c, and the wall, R_w, are shown in Fig. 4a, along with the position of a one-dimensional flame with no boundary effects, R_{1D}. The curve R_c closely follows R_{1D} until about 0.3 ms. Initially, R_w is less than R_{1D}, but this reverses at about 0.55 ms. These quantities may be converted into flame velocities in the laboratory system, V_c, shown in Fig. 4b. The one-dimensional velocity V_{1D} levels off to a constant value, but both V_c and V_w are still increasing by the time the flame reaches at the end of the channel.

The boundary-layer thickness δ_{99} is defined as the height above the wall where u reaches 99% of the centerline value. Profiles of δ_{99} as a function of time at a given value of x (not shown) indicate that the unreacted boundary layer, at a given location ahead of the flame, grows in time. This boundary layer continues to grow until the flame reaches it and destroys it. The growth is at first rapid, then it slows. The local growth is self-similar, as described by Stokes's first problem.

Figure 5 shows δ_{99} written as a function of the local time t_x, defined as the time from when the initial pressure wave, traveling at the local speed of sound in the unburned gas, reaches x. Here $t_x = t - (x - 0.3)/\sqrt{(\gamma RT_u/M)}$, where R is the specific gas

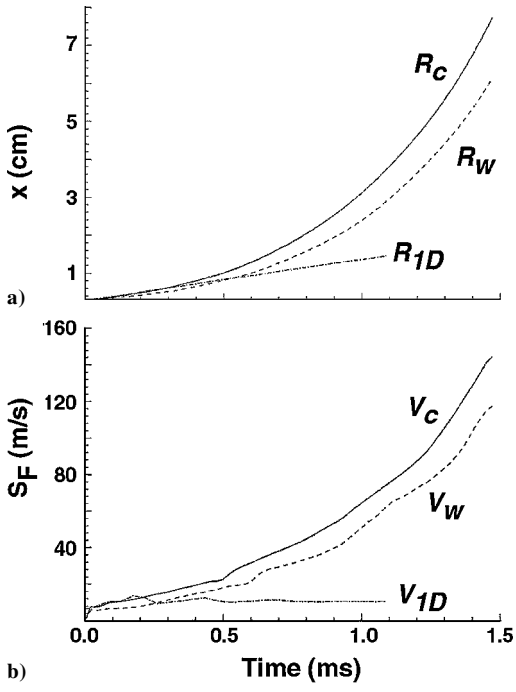

Fig. 4 Adiabatic walls: a) flame position (computed from 1000K contour) as a function of time, centerline R_c, wall R_w, and one-dimensional value R_{1D}; and b) flame propagation velocity S_F (in the laboratory coordinate system) as a function of time, centerline V_c, wall V_w, and one-dimensional value V_{1D}.

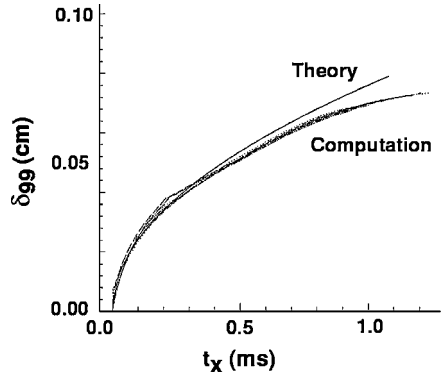

Fig. 5 Adiabatic walls; boundary-layer thickness δ_{99} as a function of reduced local time t_x comparing theoretical curve to curves derived from renormalizing the computed data at seven locations: 5.0, 5.5, 6.0, 6.5, 7.0, 7.5, and 8.0 cm.

constant, M is the molecular weight, and T_u is the unburned gas temperature. The 0.3 is needed because the initial high-temperature region used to initialize the flame was located up to 0.3 cm, so that this is where the initial pressure wave is formed. The solid line is the theoretical results from Stokes's first problem (see Refs. 1, 2, and 20), which gives $\delta_{99} = 3.64\sqrt{(\nu_u t_x)}$. In the theory, it was assumed that ν_u is held constant at the unburned gas condition and that u is constant.

The boundary-layer growth initially follows Stokes's first problem, but it then slows due to two effects acting together. The primary cause of this lowered growth rate is that the flow velocity ahead of the flame is not constant, but increases in time for all channel locations ahead of the flame. When the central flow velocity accelerates, the boundary-layer growth is slowed compared to what it would be for a constant velocity flow. The secondary cause is due to the change in viscosity ν in the unburned gas. The theory assumes ν is constant at the initial conditions of the unburned gas. The pressure waves that are generated as the flame propagates down the channel cause a decrease in the value of the kinematic viscosity in the unburned gas. The pressure wave increases the temperature and density above the initial values. The relative increase in density is greater than the relative increase in temperature. The greater rise in density lowers the kinematic viscosity. Because the boundary-layer growth is proportional the square root of the kinematic viscosity, a lower value gives a slower boundary-layer growth.

Thus, there are then two effects that combine to increase the flame propagation velocity as measured in the laboratory coordinate system. The first is the effective decrease in the channel height due to the growing boundary layer. The second is the additional momentum the flame front feels from the expansion of burned boundary-layer material. The u contours (Fig. 3c) show lower velocities in the boundary layer and higher velocity at the center of the channel. The v contours (Fig. 3d) show the fountain behind the flame front. (In this adiabatic-wall case, contours of temperature, density, and Y essentially follow each other, and therefore, only temperature contours are shown.)

Opposite Limit: Isothermal Walls

In some ways, this flow is more complex than the case of adiabatic wall. The energy loss at the walls induces a backward flow. The boundary-layer material still turns and jets upward as it burns, but now it can turn in two directions, both upstream and downstream. The result is that the flame either accelerates less than it does in the adiabatic-wall case or can even decelerate. This deceleration generates expansion waves that create an adverse pressure gradient in the boundary layer, which causes flow reversal. Effects that tend to accelerate the flame, such as the effective channel narrowing due to the creation of the boundary layer, are countered by the reverse flow behind the flame. The net result is an oscillating motion. This process is now discussed in more detail.

The profiles of flame position and propagation velocity in Fig. 6 may be compared to those in Fig. 4. Compared to the adiabatic-wall case, the flame takes considerably longer to exit the channel and the propagation velocity never reaches such high values. Also, the flame accelerates and decelerates as it propagates, which is consistent with the "jerky" motion observed in experiments.[3,5] The mean location and velocity of the flame are close to that of the one-dimensional flame.

Temperature and instantaneous flow streamlines at selected time are shown in Fig. 7. There is a large qualitative difference between

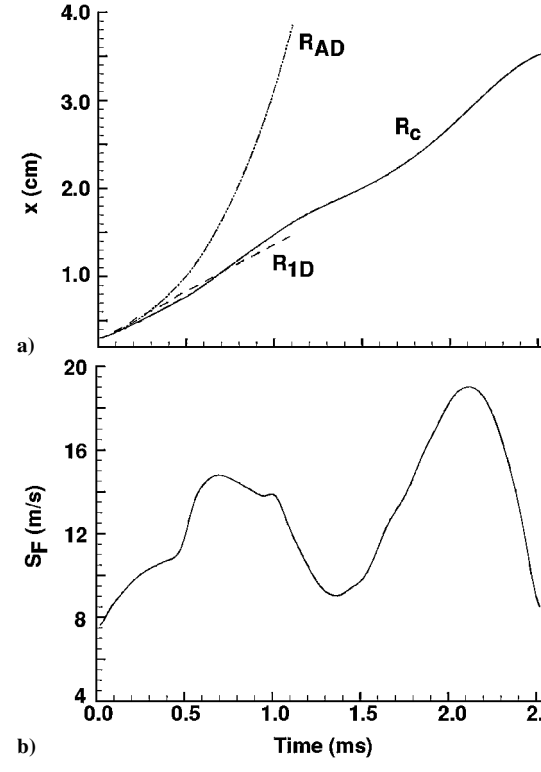

Fig. 6 Isothermal walls: a) flame position (computed from 1000K contour) as a function of time, centerline R_c, centerline from adiabatic-walls computation R_{AD}, and one-dimensional value R_{1D}; and b) flame propagation velocity S_F (in the laboratory coordinate system) at centerline.

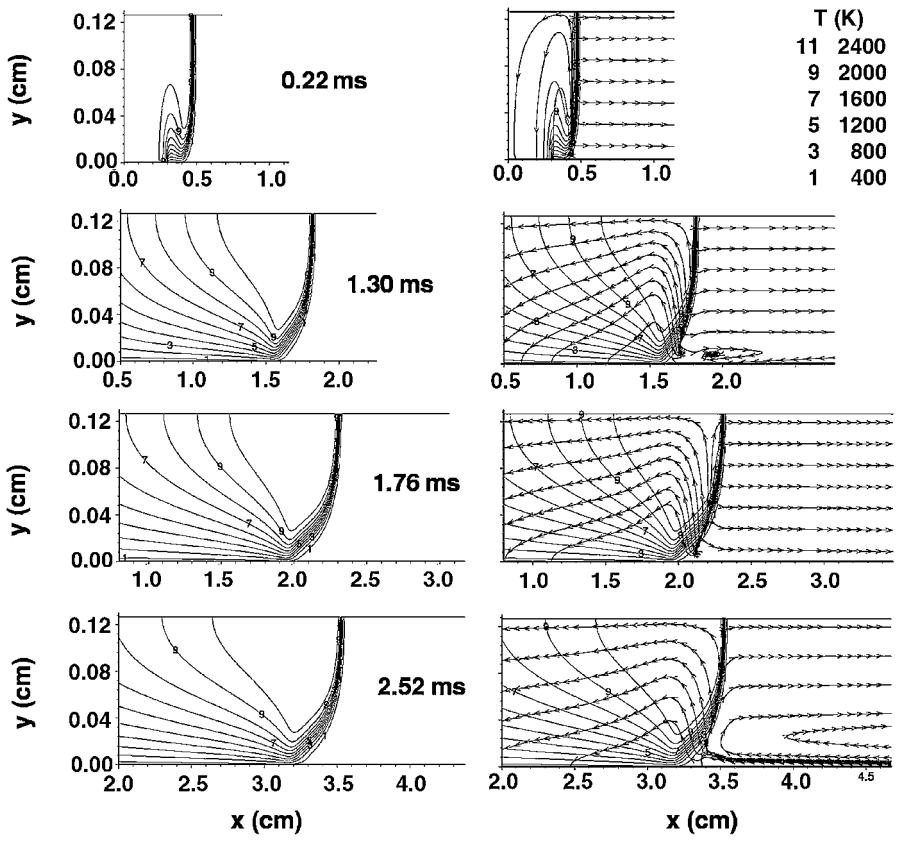

Fig. 7 Isothermal walls: a) composite of temperature contours and b) instantaneous streamlines superimposed on temperature at selected times. Temperature contours as described earlier.

the temperature profiles here and in the adiabatic-wall problem. The superposition of streamlines and temperature profiles show how the boundary-layer material jets upward and turns in both directions as it approaches the mirror process at the centerline. The wall cooling requires that the density increase to maintain essentially constant pressure. This induces motion counter to the direction of flame propagation. Figures 7 also show the development of the reverse flow in the boundary layer. Figure 6b shows that, at 0.22 and 1.76 ms, the flame is accelerating. At 1.30 and 2.50 ms, the flame is decelerating. The pressure profiles (not shown) show that, for accelerating flames, the pressure decreases ahead of the flame and that, for decelerating flames, the pressure increases.

The chemical energy release, the energy transferred from zero-point energy pqY to sensible energy $\rho c_v T$ during the chemical reaction, may be written as $\Delta E_c = \rho q(\mathrm{d}Y/\mathrm{d}t)$. The energy-release profiles (not shown) indicate that the flame is quenched near the wall. The quenching distance is defined as the smallest plate separation (in this case, channel height) that will allow the flame to propagate. This can be calculated by equating the heat generated due to chemical reactions q_c to the heat lost at the wall q_w (Refs. 21 and 22). From this definition, it can be shown that the quenching distance for a flame traveling between parallel plates[1,2] is

$$d_q = \delta_t \sqrt{2\left(\frac{k_w}{k}\right)\left(\frac{T_q - T_u}{T_b - T_u}\right)}$$

where d_q is the quenching distance, T_q is a quenching temperature, and k is the thermal conduction coefficient. Here T_q is the lowest temperature at which the flame can propagate.

Now, for example, by considering the results at 0.217 s, using a value of 1000 K for the quenching temperature, and evaluating k at the average flame temperature of 1319 K, we find that the theoretical quenching distance is 0.011 cm. Again, with the 1000 K isotherm used as a reference, the average separation distance over the entire calculation between the wall and the nearest position of the isotherm to the wall is 0.005 cm. Because this value represents quenching for half of the flame, due to the symmetry condition at the centerline, the total quenching distance is 0.010 cm, about a 10% difference from the theoretical value. This is not surprising because the evaluation of d_q as twice the dead space gives a lower bound on d_q. It has been shown[9] that for cold, isothermal walls, the dead space is about $6S_L$, where S_L is the laminar flame speed, but d_q determined as the condition for total extinguishement is nearly $15S_L$. Thus, the results presented here are consistent with experiments.[9]

Summary of Other Calculations

The computations shown earlier were two of many cases computed, described in Ref. 1. Some of these tested resolution and numerical method (mentioned earlier), all to ensure that the phenomena observed were physical. Other tests on the adiabatic wall problem were of three types: parametric studies of the effects of changing molecular diffusion or viscosity coefficients, the effects of varying the height of the tube, and the effects of varying the initial flame geometry. Note that the phenomena shown are independent of resolution and scale appropriately for the different values of viscosity and molecular diffusion. There are, however, important qualitative differences if the channel is too high, where there is less impact of the reacted boundary-layer material.

Summary

The interactions of a laminar flame propagating from the closed to the open end of a small rectangular channel were studied by solving the two-dimensional, reacting, Navier–Stokes equations with a simplified chemical model of the stoichiometric reaction of acetylene and air. These calculations describe a possibly useful mechanism of accelerating flames in small channels and explain certain phenomena previously observed as flames propagate in tubes.

More specifically, the results presented here contrast the flow structures that evolve when the boundary conditions are in the two limits, adiabatic and isothermal. All of the simulations show

boundary layers developing ahead of the flame. The flame propagates into this self-induced boundary layer, the boundary-layer material burns, and this burned material turns from the wall and is directed into the center of the channel. The subsequent effects of this jetting are both qualitatively and quantitatively different for the two different boundary conditions.

In the case of adiabatic walls, two mechanisms conspire to accelerate the flame to high velocities in the laboratory frame of reference. The first mechanism is that the channel is effectively narrowed by the growth of the boundary layer. The second mechanism is the way in which the boundary-layer material burns: It is jetted into the main body of the reacted material, where it is forced to turn and act as a piston that accelerates the flame. The growth of the boundary layer is found to be self-similar, which agrees with prediction of Stokes's first problem.

Note that the high speed of the flame is measured relative the the laboratory coordinate system. The laminar flame speed is *not* 160 m/s! Rough estimates of the laminar flame speed show that it has not increased very much (if at all) during the process described. The speed of the flame in the laboratory system is what has increased, as well as the outflow velocity and the effective thrust such a system would impart.

The flow with isothermal walls is more complex. The energy loss at the walls induces backward flow behind the flame. The boundary-layer material still turns and jets into the channel as it burns, but now it can turn in two directions, both upstream and downstream. The result is that the flame accelerates less than it does in the adiabatic-wall case, and at times, it even decelerates. This creates an adverse pressure gradient in the boundary layer. Effects that tend to accelerate the flame, such as the effective channel narrowing due to the creation of the boundary layer, are countered by the reverse flow behind the flame. The net result is that the flame oscillates as it moves down the channel. Because of the heat loss at the walls, a quench distance can be defined. The computed quench distance is consistent with a simplified theoretical analysis.

Acknowledgments

This work was sponsored by NASA and the Office of Naval Research. The computations were performed through grants from the Department of Defense High Performance Computing Modernization Office. The authors acknowledge the help of James Holdeman, Alexei Khokhlov, and Moshe Matalon. This work is part of the Ph.D. dissertation of James D. Ott.

References

[1]Ott, J. D., "The Interaction of a Flame and Its Self-Induced Boundary Layer," Ph.D. Dissertation, Dept. of Aerospace Sciences, Univ. of Maryland, 1999.

[2]Ott, J. D., Oran, E. S., and Anderson, J. D., Jr., "The Interaction of a Flame and Its Self-Induced Boundary Layer," NASA CR-1999-209401, 1999.

[3]Mallard, E., and Le Chatelier, H. L., "Recherches Expérimenteles et Théoriques sur la Combustion des Mélanges Gazeux Explosifs," *Les Annales des Mines*, 8th Ser., Vol. 4, 1883, pp. 274–335.

[4]Schmidt, E. H. W., Steinicke, H., and Neubert, U., "Flame and Schlieren Photographs of Combustion Waves in Tubes," *Proceedings of the Combustion Institute*, Vol. 7, 1970, pp. 658–667.

[5]Guénoche, H., "Flame Propagation in Tubes in Closed Vessels," *Nonsteady Flame Propagation*, edited by G. H. Markstein, Pergamon, New York, 1964, Chap. E, pp. 107–135.

[6]Kerampran, S., Desbordes, D., and Veyssière, B., "Study of the Mechanisms of Flame Acceleration in a Tube of Constant Cross-Section," *Combustion Science and Technology*, Vol. 158, 2000, pp. 71–83.

[7]Kerampran, S., Desbordes, D., Veyssiére, B., and Bauwens, L., "Flame Propagation in a Tube from Closed to Open End," AIAA Paper 2001-1082, Jan. 2001.

[8]Daou, J., and Matalon, M., "Flame Propagation in Poiseuille Flow under Adiabatic Conditions," *Combustion and Flame*, Vol. 124, 2001, pp. 337–349.

[9]Daou, J., and Matalon, M., "Influence of Conductive Heat-Losses on the Propagation of Premixed Flames in Channels," *Combustion and Flame*, Vol. 128, 2002, pp. 321–339.

[10]Brailovsky, I., and Sivashinsky, G. I., "Momentum Loss as a Mechanism for Deflagration-to-Detonation Transition," *Combustion Theory and Modelling*, Vol. 2, 1998, pp. 429–447.

[11]Kagan, L., and Sivashinsky, G. I., "The Transition from Deflagration to Detonation in Thin Channels," *Combustion and Flame* (submitted for publication).

[12]Khokhlov, A. M., Oran, E. S., Chtchelkanova, A. Y., and Wheeler, J. C., "Interaction of a Shock with a Sinusoidally Perturbed Flame," *Combustion and Flame*, Vol. 117, 1999, pp. 99–116.

[13]Khokhlov, A. M., Oran, E. S., and Thomas, G. O., "Numerical Simulation of Deflagration-to-Detonation Transition: The Role of Shock–Flame Interactions in Turbulent Flames," *Combustion and Flame*, Vol. 117, 1999, pp. 323–339.

[14]Khokhlov, A. M., and Oran, E. S., "Numerical Simulation of Detonation Initiation in a Flame Brush: The Role of Hot Spots," *Combustion and Flame*, Vol. 119, 1999, pp. 400–416.

[15]Oran, E. S., and Boris, J. P., *Numerical Simulation of Reactive Flow*, 2nd ed., Cambridge Univ. Press, Cambridge, England, U.K., 2001.

[16]Vuillermoz, P., and Oran, E. S., "Mixing Regimes in a Spatially Confined Two-Dimensional Compressible Mixing Layer," *Proceedings of the Royal Society of London, Series A: Mathematical and Physical Sciences*, Vol. 449, 1995, pp. 351–380.

[17]Weber, Y. S., Oran, E. S., Boris, J. P., and Anderson, J. D., Jr., "The Numerical Simulation of Shock Bifurcation near the End Wall in a Shock Tube," *Physics of Fluids*, Vol. 7, 1995, pp. 2475–2488.

[18]Poinsot, T., and Lele, S., "Boundary Conditions for Direct Simulations of Compressible Viscous Flows," *Journal of Computational Physics*, Vol. 101, 1992, pp. 104–129.

[19]Thompson, K., "Time-Dependent Boundary Conditions for Hyperbolic Systems," *Journal of Computational Physics*, Vol. 68, 1987, pp. 1–24.

[20]White, F. M., *Viscous Fluid Flow*, 2nd ed., McGraw–Hill, New York, 1991.

[21]Kuo, K. K., *Principles of Combustion*, Wiley, New York, 1986.

[22]Turns, S. R., *An Introduction to Combustion, Concepts and Applications*, McGraw–Hill, New York, 1996.

G. M. Faeth
Former Editor-in-Chief

Restatement of the Spalart–Allmaras Eddy-Viscosity Model in Strain-Adaptive Formulation

T. Rung,* U. Bunge,* M. Schatz,* and F. Thiele†
Technical University of Berlin,
D-10623 Berlin, Germany

I. Introduction

THE simulation of industrial aerodynamic flows is mostly based on algebraic, one- or two-equation eddy-viscosity models. For highly computing-time-consumptive applications, such as the examination of unsteady flow phenomena around three-dimensional configurations, the one-equation modeling framework is a viable compromise balancing computational effort and predictive accuracy. The Note outlines an effort to extent the predictive realms of the popular Spalart–Allmaras (SA) one-equation model[1] toward nonequilibrium conditions, by means of sensitizing the production term to nonequilibrium effects. The adopted modifications are validated for a range of engineering turbulence-modeling applications.

II. Eddy-Viscosity Transport Model

The proposed strain-adaptive linear Spalart–Allmaras (SALSA) model complies in most parts with the original SA model. The

Received 24 July 2002; revision received 14 January 2003; accepted for publication 15 January 2003.

*Research Associate, Hermann-Föttinger-Institut für Strömungsmechanik.

†Professor, Hermann-Föttinger-Institut für Strömungsmechanik.